Progress In Electromagnetics Research B, Vol. 35, 287–306, 2011

AERIAL DEGREES OF FREEDOM OF PARASITIC ARRAYS FOR SINGLE RF FRONT-END MIMO TRANSCEIVERS

V. I. Barousis* **and A. G. Kanatas**

Department of Digital Systems, University of Piraeus, 80 Karaoli & Dimitriou St., Piraeus 18534, Greece

Abstract—The beamspace domain of parasitic antenna arrays is explored in this paper, providing the aerial degrees of freedom available for use in Multiple Input-Multiple Output (MIMO) systems. The beamspace representation allows for the design of an alternative MIMO architecture based on single radio-frequency (RF) chains, and facilitates the inclusion of MIMO transceivers in devices with strict size limitations. A three dimensional orthogonal expansion is performed on the beamspace domain providing the basis patterns used for mapping of the transmitted symbols and for sampling at the receiver. The expansion is based on the Gram-Schmidt orthonormalization procedure and can be generalized for any parasitic antenna array. The multiplexing capability of ESPAR antennas is presented as a means for supporting future performance demanding communication systems. Performance evaluation results are illustrated in detail.

1. INTRODUCTION

The ever growing demand in the data rate of wireless communications systems has inevitably led the research to the application of Multiple-Input-Multiple-Output (MIMO) technology in mobile terminals. The implementation of multiple antennas and RF chains in compact devices is a hot research topic and a major challenge for the years to come [1–5]. The current perspective is based on the long experienced limitations imposed by the physical size of the terminals [1, 6]. The first limitation comes from the finite volume available for antenna implementation in the terminal. The second one is the spatial correlation and electromagnetic coupling, which reduce the available Degrees of

Received 29 September 2011, Accepted 22 October 2011, Scheduled 1 November 2011

* Corresponding author: Athanasios G. Kanatas (kanatas@unipi.gr).

Freedom (DoFs) of the antenna array. To these drawbacks, the remarkable implementation burden of conventional MIMO transceivers due to the need for multiple chains should also be considered.

An alternative novel perspective that breaks through the conventional MIMO paradigm has been proposed recently [7–10]. In particular, MIMO transmission over the air is achieved [11] with the use of antenna arrays that consist of only a single active element, surrounded by a number of passive (parasitic) neighboring antennas. The parasitic antennas, as has been long understood, carry currents that are induced on them via their strong mutual coupling with the neighboring active element [12–16]. The induced currents depend on the array topology and can be controlled via low cost analogue circuits, e.g., varactors, to provide beamforming capabilities [17–19]. An example of such a parasitic antenna is shown in Fig. 1. In [20] and then in [21] and [7] it was clearly shown that parasitic antenna arrays preserve the capability to also perform MIMO transmission. The MIMO functionality is presented at the *beamspace domain* [22, 23]. In transmitting mode, symbols are not driven to diverse active antenna elements as in conventional case, but they modulate orthogonal radiation patterns, providing the term *aerial modulation*. The receiver in turn assesses the impinging signals by switching among orthogonal patterns within a symbol period [8, 10]. To emphasize the principle of operation, the complete functionality is called *Beamspace MIMO* (BS-MIMO).

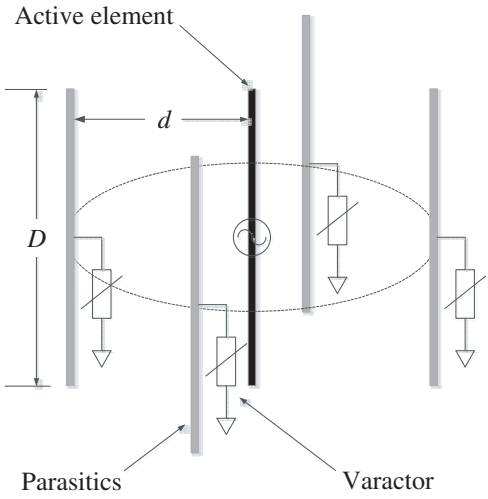

Figure 1. Circular ESPAR with 5 elements.

This paper provides an analytical treatment of the *aerial degrees of freedom* (ADoFs) available for MIMO transmission with parasitic antenna arrays. Similar to the spatial multiplexing factor of conventional MIMO systems, these DoFs show the potential of parasitic antenna arrays to achieve a linear increase of spectral efficiency over the air; the difference now being that this increase is obtained in the beamspace domain, as opposed to the antenna domain of conventional MIMO. The effective number of DoFs of MIMO channels has been investigated using the spatial Nyquist intervals and the spatial sampling theory in [24, 25]. Moreover, based on the theory of non-redundant sampling of the electromagnetic field [26, 27] provide invaluable results on the DoF of the radiated field in MIMO channels. In [38] the authors analyze the interaction between antennas and the propagation channel and study both the antennas and the propagation channel by means of the spherical vector wave mode expansion of the electromagnetic field. They also prove that the optimum decorrelation of the antenna signals is obtained by the excitation of orthogonal spherical vector modes. In [39] the authors present some examples of uncorrelated antenna radiation patterns for MIMO applications. In this paper we follow the notion of DoF provided in [25] and [28], but in the beamspace domain, where the spatial sampling theory is not applicable due to the parasitic elements. Indeed, the DoFs of the Electrically Steerable Passive Array Radiator (ESPAR) antennas are explored by providing the expansion of the far field pattern in a complete set of orthonormal basis functions. A generalized methodology for the calculation of the available DoFs is given for ESPAR antennas, irrespective of the channel conditions and the noise level. In other words, the possible multiplexing capabilities of the antenna are explored and an extended discussion is provided on the effects of antenna array dimensions on the *effective DoFs* (EDoFs). The remainder of the paper is organized as follows: Section 2 presents a brief review of BS-MIMO representation and sets the starting point for the beamspace representation of ESPAR antennas. Section 3 provides a generalized methodology for the calculation of the aerial DoFs of ESPAR antennas. The methodology is based on the well known Gram-Schmidt orthonormalization procedure [29], which provides a 3D orthogonal expansion of the beamspace domain. Analytic results are given as application examples for a circular 5-element ESPAR antenna. Next, Section 4 discusses the effect of the array dimensions on the number of EDoFs that are available for specific design parameters. Section 5 illustrates the performance of the proposed scheme in terms of capacity achieved in a full scattering environment. Finally, Section 6 summarizes the key findings of the paper.

2. BEAM SPACE DOMAIN ANALYSIS OF SINGLE RF MIMO SYSTEMS

The limitation of a single active element does not allow for the assignment of diverse transmit symbols to different antenna elements and therefore, known spatial signal processing techniques for MIMO transmission cannot be used directly. The question now is how to transmit different signals simultaneously with a single active element. The answer lies in the beamspace domain representation of parasitic antenna arrays. This representation has been already considered for the study of antenna arrays [30], as well as for the intuitive modeling of MIMO channels [22, 23]. The author in [22] proposes an alternative MIMO channel representation in terms of angular basis functions or "eigen-patterns", thus the MIMO channel matrix is defined at the beamspace or angular domain. The beamspace domain of an antenna array is a signal space where any radiation pattern of the antenna can be represented by a point within that space with position vector whose coordinates correspond to the basis patterns which are mutually orthogonal. Apparently, increasing the dimensions of the beamspace domain, i.e., the number of aerial DoFs, the beamforming capabilities of the antenna become stronger. In contrast to conventional MIMO transmitters, in the single RF MIMO transmitter each symbol is allocated to a basis pattern. Thus, the number of symbols that can be simultaneously transmitted is restricted by the aerial DoFs of the parasitic antenna array. At the receiver, the spatial sampling of the incident waves is not feasible and samples are obtained at the beamspace domain using the available basis patterns [10]. The narrowband signal model can be written [10]

$$\mathbf{y}_{bs} = \mathbf{H}_{bs}\mathbf{s}_{bs} + \mathbf{n}_{bs} = \mathbf{\Phi}_R^H \mathbf{H}_b \mathbf{\Phi}_T \mathbf{s}_{bs} + \mathbf{n}_{bs} \tag{1}$$

where $\mathbf{y}_{bs}$ is the received signal vector that contains samples of the transmitted symbols, $\mathbf{s}_{bs}$, as these are obtained using different basis patterns. The elements of the channel matrix $\mathbf{H}_{bs}$ correspond to the complex channel gains among the basis patterns of the transmitter and receiver parasitic arrays. This matrix can be written with the help of a parametric physical model that considers the geometry of the scattering environment and the basis patterns at the transmitter and the receiver as $\mathbf{H}_{bs} = \mathbf{\Phi}_R^H \mathbf{H}_b \mathbf{\Phi}_T$. In this representation each path i connecting the area of the transmitter with the area of the receiver has a single direction-of-departure (DoD) $\Omega_{T,i}$ and a single direction-of-arrival (DoA) $\Omega_{R,i}$, and a path gain b_i. For M_T aerial DoFs or equivalently basis patterns at the transmitter, the matrix $\mathbf{\Phi}_T(K \times M_T)$ contains M_T column vectors with samples of the basis patterns towards the DoDs. The same applies to the matrix $\mathbf{\Phi}_R$ $(K \times M_R)$ that contains

M_R vectors with samples of the basis patterns towards the DoAs. If K paths exist, then $\mathbf{H}_b$ is a diagonal $(K \times K)$ matrix whose entries represent the complex gain of each path. With these in mind, the functionality of single RF MIMO Tx and Rx are explained at the beamspace domain in more detail.

2.1. Single RF MIMO Transmitter

If the radiated pattern at the transmitter can be expressed as a linear combination of the basis patterns with weights that correspond to the transmitted symbols, then $P_T(\theta, \varphi)$ is a vector with angular samples of the radiated pattern and is written as

$$P_T(\theta, \varphi) = \mathbf{\Phi}_T \mathbf{s}_{bs} = \sum_{n=0}^{M_T-1} s_{bs,n} \Phi_n(\theta, \varphi) \tag{2}$$

where $\Phi_n(\theta, \varphi)$ is the n-th basis pattern of the parasitic array at the transmitter. Equation (2) states that at each symbol period the shape of the radiated pattern, i.e., its amplitude and phase components, is determined by the symbol vector $\mathbf{s}_{bs}$ for transmission. Indeed, each transmit symbol modulates a different basis pattern, an operation that can be thought of as pattern mapping, or aerial modulation.

2.2. Single RF MIMO Receiver

At the single RF MIMO receiver, the simultaneous reception of multiple signals at the spatial domain is not possible. Signals have to be obtained at the beamspace domain using all possible basis patterns *serially*, i.e., in a time division mode, during the same symbol period. This is accomplished by splitting the symbol period to sub-periods, the number of which is identical to the number of available basis patterns, i.e., the number of available aerial DoFs. At each sub-period the impinging signals are assessed using one of the basis patterns. The oversampling of the impinging signals within the symbol period has a negative effect on the system performance as compared to conventional MIMO transceivers, since reduces the effective SNR by the oversampling factor, i.e., by the number of pattern switching within a symbol period. This drawback has been pointed out in [8] and [10].

3. 3D PATTERN ORTHOGONAL EXPANSION

The objective in this section is to provide a methodology for the calculation of the available DoFs for a general category of parasitic

arrays, the ESPAR antennas [15]. This objective is achieved with the decomposition of the far field ESPAR pattern to orthonormal functions, called *basis patterns*. An ESPAR with M elements consists of a single active element surrounded by $M-1$ parasitic elements, often called *parasitics*, usually in linear or circular arrangement. Fig. 1 shows a circular ESPAR antenna with $M=5$ elements. Due to strong mutual couplings, the feeding of the active element is responsible for the currents induced to all parasitics and beamforming is possible by adjusting the connected variable loads [19]. The current vector is given by $\mathbf{i} = v_s(\mathbf{Y}^{-1} + \mathbf{X})^{-1}\mathbf{u}$, where $\mathbf{Y}$ is the $(M \times M)$ admittance matrix, obtained using an antenna analysis software, with each entry y_{ij} representing the mutual admittance between the i-th and j-th element. The load matrix $\mathbf{X} = \text{diag}[\ 50 \quad jx_1 \quad \dots \quad jx_{M-1}\ ]$, adjusts the radiation pattern, whereas $\mathbf{u} = [\ 1 \quad 0 \quad \dots \quad 0\ ]^T$ is a $(M \times 1)$ column selection vector and v_S is the complex feeding at the active element [16]. The radiation pattern is then given by:

$$P(\theta,\varphi) = \mathbf{i}^T\mathbf{a}(\theta,\varphi) = \sum_{m=0}^{M-1} i_m a_m(\theta,\varphi) \tag{3}$$

where $\mathbf{a}(\theta,\varphi) = [\ a_0(\theta,\varphi) \quad \dots \quad a_{M-1}(\theta,\varphi)\ ]^T$ is the steering vector of the ESPAR at a direction (θ,φ). The relationship between the radiation pattern and the loading matrix is non-linear. Consequently, it is preferable to study the radiation capabilities of ESPAR antennas by considering the antenna geometry indirectly. The beamspace representation approach bypasses the nonlinear ESPAR equations and describes the radiation mechanism using more tractable expressions.

3.1. Gram-Schmidt Method for Arbitrary Planar ESPAR Geometry

To represent $P(\theta,\varphi)$ at the beamspace domain, the functions $a_m(\theta,\varphi),\ m=0,\dots,M-1$ are expressed as a linear combination of orthonormal functions $\Phi_n(\theta,\varphi),\ n=0,\dots,N-1$, that span a N-th dimensional space. For this purpose the process of Gram-Schmidt orthonormalization is used [29]. This process accepts a set of M linearly independent functions and provides a set of $N \leq M$ orthonormal functions that span an N-dimensional space, i.e., $a_m(\theta,\varphi) = \sum_{n=0}^{N-1} q_{mn}\Phi_n(\theta,\varphi)$. Therefore:

$$P(\theta,\varphi) = \sum_{m=0}^{M-1} i_m \sum_{n=0}^{N-1} q_{mn}\Phi_n(\theta,\varphi), \quad N \leq M \tag{4}$$

where $q_{mn} = \int_0^{2\pi}\int_0^{\pi} a_m(\theta,\varphi)\Phi_n^*(\theta,\varphi)\sin\theta d\theta d\varphi$, denotes the projection of $a_m(\theta,\varphi)$ onto the basis pattern $\Phi_n(\theta,\varphi)$. The steering vectors for an arbitrary planar ESPAR geometry are:

$$a_m(\theta,\varphi) = \begin{cases} 1 & m = 0 \\ \exp\left[jb_m \sin\theta\cos(\varphi-\varphi_m)\right] & m \neq 0 \end{cases} \tag{5}$$

where φ_m represents the angle of the m-th parasitic element in the azimuthal plane with respect to a reference axis, $b_m = 2\pi d_m$, and d_m is the normalized to the wavelength distance of the m-th parasitic from the active element. Observing (2) for $b_m \neq 0$, all functions $a_m(\theta,\varphi)$ are linearly independent implying that $N = M$ [29]. Thus, the aerial DoFs theoretically equal the number of ESPAR elements and

$$\begin{aligned} P(\theta,\varphi) &= \sum_{m=0}^{M-1} i_m \sum_{n=0}^{M-1} q_{mn}\Phi_n(\theta,\varphi) = \sum_{n=0}^{M-1}\sum_{m=0}^{M-1} i_m q_{mn}\Phi_n(\theta,\varphi) \\ &= \sum_{n=0}^{M-1} \mathbf{i}^T\mathbf{q}_n\Phi_n(\theta,\varphi) = \sum_{n=0}^{M-1} s_{bs,n}\Phi_n(\theta,\varphi) \end{aligned} \tag{6}$$

where $\mathbf{q}_n = \begin{bmatrix} q_{0n} & \cdots & q_{(M-1)n} \end{bmatrix}^T$ is a $(M \times 1)$ vector with the projections of all functions $a_m(\theta,\varphi)$, $m = 0,\ldots,M-1$ onto $\Phi_n(\theta,\varphi)$. From (3) the n-th basis pattern is weighted by the symbol $s_{bs,n} = \mathbf{i}^T\mathbf{q}_n$ and $\mathbf{s}_{bs} = \begin{bmatrix} s_{bs,0} & s_{bs,1} & \cdots & s_{bs,M-1} \end{bmatrix}^T$ defines a coordinate vector at the beamspace domain which corresponds to a radiated pattern. Gram-Schmidt process begins by selecting any function $a_m(\theta,\varphi)$. Starting from $a_0(\theta,\varphi)$, the first basis pattern is $\Phi_0(\theta,\varphi) = a_0(\theta,\varphi)/k_0$, while the remaining are obtained by subtracting out the projection of the next function onto the functions defined so far in the orthonormal set:

$$\Phi_n(\theta,\varphi) = \frac{1}{k_n}\left(a_n(\theta,\varphi) - \sum_{s=0}^{n-1} q_{ns}\Phi_s(\theta,\varphi)\right) \tag{7}$$

where $k_n = \sqrt{\int_0^{2\pi}\int_0^{\pi} |a_n(\theta,\varphi) - \sum_{s=0}^{n-1} q_{ns}\Phi_s(\theta,\varphi)|^2 \sin\theta d\theta d\varphi}$, $n = 0,\ldots,N-1$, are the normalization coefficients ensuring basis patterns with unit power. For an arbitrary geometry and number of parasitic elements the basis patterns can be computed numerically by the iterative expression (7). It will be shown in Section 4 that not necessarily all the DoFs are effective, especially for all geometries and

antenna dimensions. Having decided upon the number of DoFs to be exploited as well as the type of modulation scheme to be used in a MIMO system, (9) implies that one can calculate all the possible linear combinations, i.e., all the patterns to be radiated. For a specific ESPAR antenna it is then possible to calculate the set of load matrices $\mathbf{X}$ that will provide the required patterns [18].

3.2. Analytic Results for 5 Element Circular ESPAR

Next, the Gram-Schmidt process is applied to the circular ESPAR with 5 elements shown in Fig. 1. The selected ESPAR configuration has been reported as the simplest one that supports 360° beam steering, thus allowing for high beamforming capabilities [15]. The circular arrangement of the parasitics implies that $b_m = b = 2\pi d$ where d denotes the antenna radius normalized to the wavelength, while $\varphi_m = (m-1)\,2\pi/(M-1),\ m = 1,\dots M-1$. Substituting to (3) the radiation pattern becomes:

$$\begin{aligned} P(\theta,\varphi) &= i_0 + i_1 e^{jb\sin\theta\cos\varphi} + i_2 e^{jb\sin\theta\cos\varphi} + i_3 e^{-jb\sin\theta\cos\varphi} + i_4 e^{-jb\sin\theta\cos\varphi} \\ &= i_0 \underbrace{1}_{\tilde{a}_0(\theta,\varphi)} + j(i_1 - i_3)\underbrace{\sin(b\sin\theta\cos\varphi)}_{\tilde{a}_1(\theta,\varphi)} + j(i_2 - i_4)\underbrace{\sin(b\sin\theta\sin\varphi)}_{\tilde{a}_2(\theta,\varphi)} \\ &\quad + (i_1 + i_3)\underbrace{\cos(b\sin\theta\cos\varphi)}_{\tilde{a}_3(\theta,\varphi)} + (i_2 + i_4)\underbrace{\cos(b\sin\theta\sin\varphi)}_{\tilde{a}_4(\theta,\varphi)} \end{aligned} \quad (8)$$

The expansion in the second part of (11) was done in order to simplify the analytical derivation. Therefore, the functions used for the orthogonal expansion in this example are the $\tilde{a}_i(\theta,\varphi)$, and not the complex exponentials of the steering vector. It is easy to show that the two solutions are equivalent. Applying the Gram-Schmidt process, the basis patterns that construct the beamspace domain are given after some mathematical manipulations (see Appendix) by:

$$\begin{aligned} &\Phi_0(\theta,\varphi) = \frac{1}{k_0} && \Phi_1(\theta,\varphi) = \frac{1}{k_1}\sin(b\sin\theta\cos\varphi) \\ &\Phi_2(\theta,\varphi) = \frac{1}{k_2}\sin(b\sin\theta\sin\varphi) && \Phi_3(\theta,\varphi) = \frac{1}{k_3}\left[\cos(b\sin\theta\cos\varphi) - \frac{q_{30}}{k_0}\right] \\ &\Phi_4(\theta,\varphi) = \frac{1}{k_4}\left[\cos(b\sin\theta\sin\varphi) - \frac{q_{40}}{k_0} - \frac{q_{43}}{k_3}\cos(b\sin\theta\cos\varphi) + \frac{q_{43}q_{30}}{k_0 k_3}\right] \end{aligned} \quad (9)$$

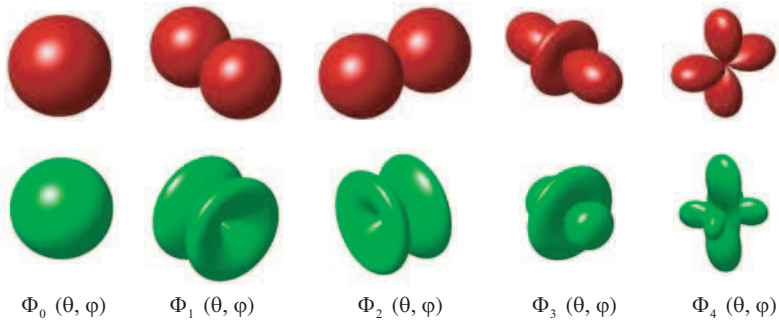

Figure 2. 3D Basis patterns of a circular ESPAR antenna with $M_T = 5$. The red patterns correspond to $d = 1/16$ and the green ones to $d = 1/2$.

where q_{mn} are the projections defined in Section 3.1 and are given by:

$$q_{30} = \frac{\pi}{k_0} \int_0^{2\pi} E_1 (b \cos\varphi) d\varphi$$

$$q_{40} = \frac{\pi}{k_0} \int_0^{2\pi} E_1 (b \sin\varphi) d\varphi \tag{10}$$

$$q_{43} = \frac{\pi}{k_3} \int_0^{2\pi} E_1 \left[2b \cos(\pi/4) \cos\varphi\right] d\varphi - \frac{q_{30} q_{40}}{k_3}$$

In (10), the function $E_1(z)$ denotes the Weber function of the first order defined as [31]:

$$E_\nu (z) = \frac{1}{\pi} \int_0^{\pi} \sin(\nu\theta - z \sin\theta) d\theta \tag{11}$$

As an example, Fig. 2 presents the basis patterns for $d = 1/16$ and $d = 1/2$.

4. EFFECTIVE AERIAL DOFS AND ARRAY DIMENSION

The presented decomposition based on Gram-Schmidt process implies that the number of aerial DoFs, i.e., the beamspace dimensionality, is equal to the number of ESPAR elements. However in this Section it is

shown that the electromagnetic coupling between the ESPAR elements, which is heavily dependent on the array's dimensions, strongly affects the subset of significant aerial DoFs $N_{eff} \leq M_T$, called effective aerial DoFs (EDoFs). A similar result has been recorded in [10], where a rough estimation of the effective aerial DoFs is shown. The authors therein consider an azimuth decomposition of the ESPAR pattern and also ignore the electromagnetic coupling between elements. To cope with this effect, the complex coupling $Z_{mn} = R_{mn} + jX_{mn}$ between two side by side elements is used as given by [31]:

$$\begin{aligned} R_{mn} &= 30\left[2C_i(2\pi) - C_i\left(2\pi\left(\sqrt{\tilde{d}_{mn}^2 + D^2} + D\right)\right) - C_i\left(2\pi\left(\sqrt{\tilde{d}_{mn}^2 + D^2} - D\right)\right)\right] \\ X_{mn} &= -30\left[2S_i(2\pi) - S_i\left(2\pi\left(\sqrt{\tilde{d}_{mn}^2 + D^2} + D\right)\right) - S_i\left(2\pi\left(\sqrt{\tilde{d}_{mn}^2 + D^2} - D\right)\right)\right] \end{aligned} \tag{12}$$

where $\tilde{d}_{mn}$ is the distance between the m-th and n-th ESPAR elements (this is not the ESPAR radius), D is the element's length, usually equal to $\lambda/2$, and $S_i(x)$, $C_i(x)$ are the sine and cosine integrals [36].

The impact of the array's dimension on the number of EDoFs is estimated indirectly. In particular, the power contribution of each basis pattern to the total radiated power is evaluated as a function of the ESPAR's radius d, which determines the distance $\tilde{d}_{mn}$ between the side by side elements, and considering also the corresponding coupling effects. Focusing on a specific radius d, 10,000 random patterns were generated by changing the loads at the parasitics randomly in the range of -100 to 100 Ohms. Then, the contribution of each basis pattern at the randomly generated patterns was computed. Fig. 3 presents the mean values over all projections, in terms of power, as a function of d. It is observed that for tiny values of d only the first basis pattern $\Phi_0(\theta, \varphi)$ dominates. Intuitively this is reasonable since with an extremely small d the array approaches the point source. Increasing the ESPAR radius, more basis patterns participate considerably to the total radiated pattern, while larger radii values reduce remarkably the contribution of all basis patterns except the first that eventually dominates. This behavior is also reasonable, since large radii values weaken considerably the electromagnetic coupling between elements. In terms of ESPAR theory this means that the currents induced on the parasitics due to feeding of the sole active element gradually attenuate, and the contribution of the parasitics to radiation mechanism is minimized. The radiation in this case is only due to the active element's feeding. Consequently, Fig. 3 constitutes a quantitative and qualitative

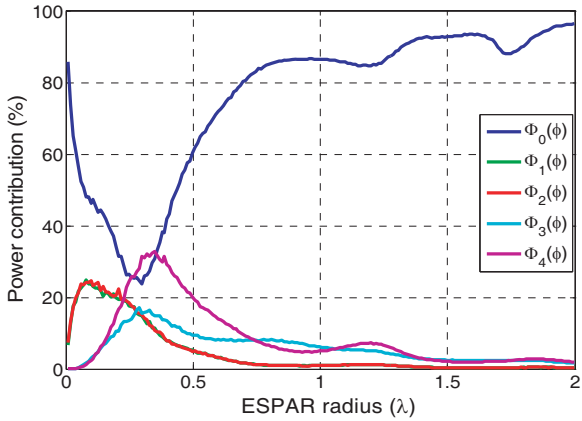

Figure 3. Mean power contributed by each basis pattern (%) to the total power.

illustration of the ESPAR features, showing that for certain radii values the contribution of all basis patterns is maximized allowing for high beamforming capabilities. What is pointed out is that an ESPAR is fully functional for small radii values. Up to now this fact has been adopted implicitly in the literature on ESPAR antennas. According to the authors' knowledge such a descriptive visualization is novel and can be applied also to ESPARs with arbitrary geometry. Therefore, although the Gram-Schmidt process indicates that the dimensionality of the beamspace domain depends only on the number of ESPAR elements, Fig. 3 illustrates the behavior of all basis patterns as a function of the radius and provides the number of EDoFs that can be actually exploited. This knowledge is of great interest when studying ESPAR antennas in a communication system level, as follows in Section 5. It should be emphasized that the singular value decomposition (SVD) method can provide an equivalent set of basis patterns that inevitably belong to the same space.

5. PERFORMANCE EVALUATION

This Section provides performance evaluation results of the proposed single RF MIMO architecture against its conventional counterpart MIMO transceivers in terms of capacity. The proposed architecture utilizes the basis patterns computed in previous section for a 5-element circular ESPAR antenna. Based on (2) and Fig. 3 it is observed that a single RF MIMO transmitter is able to create up to $N_{eff} = M_T = 5$ uncorrelated data pipes at the beamspace domain using an ESPAR

antenna with radius well below 0.5 wavelengths, i.e., $d = 0.25$. In contrast, a conventional MIMO transceiver would require much larger antenna dimensions to ensure spatially uncorrelated transmit signals and to attain the same multiplexing order. Thus, a fair comparison between the two competitive MIMO approaches would impose the same restrictions on antenna dimensions. By reducing the antenna spacing in conventional MIMO systems, two effects cause capacity degradation: the spatial correlation of transmit and receive signals and the antenna mutual couplings. This is the case in applications with critical size and cost constraints, where the available space is limited to distribute the antenna elements over. To account for these effects the conventional MIMO channel $\mathbf{H}_{conv}$ is expressed as in [10] using the Kronecker model [32] combined with the transmit and receive coupling matrices as in [33, 34]. Since a full scattering environment is considered, the correlation coefficient between the m-th and n-th antenna is evaluated as $\rho_{mn} = J_0(2\pi\tilde{d}_{mn})$, $m \neq n$ and $\rho_{mn} = 1$, $m = n$ [35], where $J_0(\cdot)$ is the zero order Bessel function of the first kind. The fair comparison of the two MIMO systems calls for the inclusion of the oversampling effect at the single RF receiver, as explained in Section 2.2. The oversampling causes SNR degradation, as compared to conventional MIMO, by the oversampling factor, i.e., by the number of pattern switching:

$$\gamma_{bs} = \gamma_{conv}/N_{eff} \tag{13}$$

where γ_{bs} and γ_{conv} denote the SNR in single RF and conventional MIMO respectively, and $N_{eff} \leq M_T$ indicates the number of EDoFs. The capacity of single RF MIMO is evaluated by:

$$C = \log_2\left(\det\left(\mathbf{I} + \frac{\gamma_{bs}}{N_{eff}}\mathbf{H}_{bs}\mathbf{H}_{bs}^H\right)\right) \tag{14}$$

The same expression applies also in conventional MIMO by replacing $\mathbf{H}_{bs}$ with $\mathbf{H}_{conv}$, γ_{bs} with γ_{conv} and N_{eff} with the number of transmit antenna elements [10, 22]. Fig. 4 illustrates the ergodic capacity of single RF MIMO when transmit and receive ESPAR antennas are able to offer $N_{eff} = 3$ or 5 EDoFs. According to Fig. 3 this is reasonable for $d = 1/16$ and $d = 1/4$ respectively. The performance is compared against the conventional counterparts, i.e., 3×3 and 5×5 MIMO, as well as the classic SISO system. The comparison against conventional MIMO is twofold; the ideal case ignores the spatial correlation of signals and any couplings between elements, provided that the antenna separation at both link ends is sufficient. On the contrary, the non-ideal case takes into account both effects, as explained. For fair comparison uniform circular arrays (UCAs) are considered in the latter case preserving the same dimensions as in single RF MIMO. It is clearly

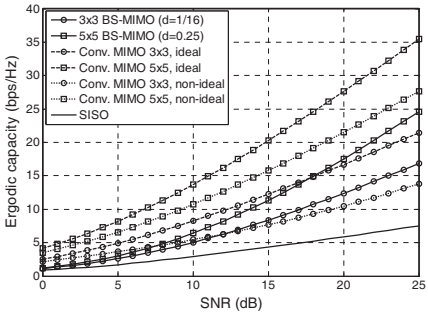

Figure 4. Single RF MIMO vs conventional MIMO (ideal and non-ideal) and SISO: Ergodic capacity comparison.

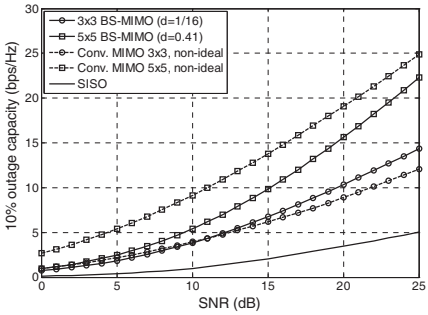

Figure 5. Single RF MIMO vs conventional MIMO (ideal and non-ideal) and SISO: 10% outage capacity comparison.

shown that ideal conventional MIMO outperform all cases. This is expected since according to (13) the oversampling factor in single RF MIMO introduces a reasonable SNR loss. Increasing the ESPAR radius the number of EDoFs becomes $N_{eff} = M_T = 5$ and the capacity also increases, but less than in ideal conventional case. This is reasonable, since the transmitting ESPAR is able to multiplex more symbols at the beamspace domain, but on the other hand the SNR degradation at the receiver reduces the capacity enhancement. The fair comparison against non-ideal conventional MIMO reveals the real benefits of single RF MIMO architecture. Although it seems that the proposed scheme is not advantageous for high MIMO order systems, in applications with stringent size limitations it's able to offer the MIMO benefits, even with increased performance as compared to the conventional counterpart. This observation is important considering also the significant hardware savings in single RF MIMO; the RF chains have been replaced with a simpler varactor-based circuit attached to the parasitics [17–19]. For completeness, Fig. 4 depicts also a comparison against the SISO system, which in terms of hardware complexity is meaningful. Fig. 5 in turn, illustrates a comparison regarding the 10% outage capacity, with similar observations. One should notice that a clustered propagation channel, will definitely affect the performance of the BS-MIMO as well as that of the conventional MIMO system [37], but will not alter the calculation of the DoFs provided by the ESPAR antenna. Finally, we should highlight that the measurement results obtained in the proof-of-concept experiment described in [11], were based on initial theoretical investigation of orthogonal or semi-orthogonal basis patterns provided in [9].

6. CONCLUSION

This paper explores the beamspace domain representation of parasitic antenna arrays and elaborates on the aerial degrees of freedom provided by these arrays. A geometry based methodology is used to visualize the multiplexing capabilities of ESPAR antennas. Although a circular ESPAR with 5 elements was used for demonstration, the methodology can be used effectively for other geometries. A key result of the paper is that with significantly reduced antenna dimensions a reasonable number of orthogonal basis patterns can be produced, able to support uncorrelated transmit signals at the beamspace domain. Therefore, the multiplexing can be done in the beamspace domain where multiple transmit symbols are mapped to different basis patterns. The results are very promising for the application of parasitic arrays in single RF MIMO transceivers with reduced hardware complexity and pave the way for lightweight MIMO systems that are well suited to mobile devices with strict size limitations.

APPENDIX A.

The circular ESPAR's radiation pattern is given in (8). As explained in Section 3, the first basis pattern is chosen as:

$$\Phi_0(\theta,\varphi) = \frac{1}{k_0} \tag{A1}$$

The projection q_{10} of $\tilde{a}_1(\theta,\varphi)$ onto $\Phi_0(\theta,\varphi)$ is computed as:

$$\begin{aligned} q_{10} &= \int_0^{2\pi}\int_0^{\pi} \tilde{a}_1(\theta,\varphi)\Phi_0^*(\theta,\varphi)\sin\theta d\theta d\varphi = \frac{1}{k_0}\int_0^{2\pi}\int_0^{\pi} \sin(b\sin\theta\cos\varphi)\sin\theta d\theta d\varphi \\ &= \frac{1}{2k_0}\int_0^{2\pi}\int_0^{\pi} \cos(b\sin\theta\cos\varphi-\theta)d\theta d\varphi - \frac{1}{2k_0}\int_0^{2\pi}\int_0^{\pi} \cos(b\sin\theta\cos\varphi+\theta)d\theta d\varphi \\ &= \frac{\pi}{2k_0}\int_0^{2\pi} J_1(b\cos\varphi)d\varphi + \frac{\pi}{2k_0}\int_0^{2\pi} J_{-1}(b\cos\varphi)d\varphi \\ &= \frac{\pi}{k_0}\int_0^{2\pi} J_1(b\cos\varphi)d\varphi = 0 \end{aligned} \tag{A2}$$

Thus, due to (7) the next basis pattern is:

$$\Phi_1(\theta,\varphi) = \frac{1}{k_1}\sin(b\sin\theta\cos\varphi) \tag{A3}$$

Therefore:

$$\Phi_2(\theta,\varphi) = \frac{1}{k_2}\left[\tilde{a}_2(\theta,\varphi) - q_{20}\Phi_0(\theta,\varphi) - q_{21}\Phi_1(\theta,\varphi)\right] \tag{A4}$$

Similarly, as in (A2) it holds that:

$$q_{20} = \int_0^{2\pi}\int_0^{\pi} \tilde{a}_2(\theta,\varphi)\,\Phi_0^*(\theta,\varphi)\sin\theta d\theta d\varphi = 0 \tag{A5}$$

The projection q_{21} is computed after long mathematical manipulations considering similar trigonometric identities and the Weber function of the first order $E_1(z)$ given in (11) as:

$$\begin{aligned} q_{21} &= \int_0^{2\pi}\int_0^{\pi} \tilde{a}_2(\theta,\varphi)\,\Phi_1^*(\theta,\varphi)\sin\theta d\theta d\varphi \\ &= \frac{1}{k_1}\int_0^{2\pi}\int_0^{\pi} \sin(b\sin\theta\sin\varphi)\sin(b\sin\theta\cos\varphi)\sin\theta d\theta d\varphi \\ &= \frac{1}{2k_1}\int_0^{2\pi}\int_0^{\pi} d\theta d\varphi \sin\theta[\cos(b(\sin\varphi-\cos\varphi)\sin\theta) \\ &\quad - \cos(b(\sin\varphi+\cos\varphi)\sin\theta)] = 0 \end{aligned} \tag{A6}$$

In (A6) we also take into account that $E_1(z) = -E_{-1}(z)$ and $E_1(z) = E_1(-z)$. Due to (A5) and (A6) the next basis pattern is:

$$\Phi_2(\theta,\varphi) = \frac{1}{k_2}\sin(b\sin\theta\sin\varphi) \tag{A7}$$

The projections of the term $\tilde{a}_3(\theta,\varphi)$ onto all basis patterns defined so far are computed similarly:

$$\begin{aligned} q_{30} &= \int_0^{2\pi}\int_0^{\pi} \tilde{a}_3(\theta,\varphi)\Phi_0^*(\theta,\varphi)\sin\theta d\theta d\varphi = \frac{1}{k_0}\int_0^{2\pi}\int_0^{\pi} \cos(b\sin\theta\cos\varphi)\sin\theta d\theta d\varphi \\ &= \frac{\pi}{k_0}\int_0^{2\pi} E_1(b\cos\varphi)d\varphi \end{aligned} \tag{A8}$$

$$q_{31} = \int_0^{2\pi}\int_0^{\pi} \tilde{a}_3(\theta,\varphi)\Phi_1^*(\theta,\varphi)\sin\theta d\theta d\varphi$$
$$= \frac{1}{k_1}\int_0^{2\pi}\int_0^{\pi} \cos(b\sin\theta\cos\varphi)\sin(b\sin\theta\cos\varphi)\sin\theta d\theta d\varphi$$
$$= \frac{1}{2k_1}\int_0^{2\pi}\int_0^{\pi} \sin(2b\sin\theta\cos\varphi)\sin\theta d\theta d\varphi = 0 \quad \text{(A9)}$$

$$q_{32} = \int_0^{2\pi}\int_0^{\pi} \tilde{a}_3(\theta,\varphi)\Phi_2^*(\theta,\varphi)\sin\theta d\theta d\varphi$$
$$= \frac{1}{k_2}\int_0^{2\pi}\int_0^{\pi} \cos(b\sin\theta\cos\varphi)\sin(b\sin\theta\sin\varphi)\sin\theta d\theta d\varphi = 0 \quad \text{(A10)}$$

Due to (7), (A8), (A9) and (A10) the next basis pattern consequently is:

$$\Phi_3(\theta,\varphi) = \frac{1}{k_3}\left[\cos(b\sin\theta\cos\varphi) - \frac{q_{30}}{k_0}\right] \quad \text{(A11)}$$

Working in the same way the last basis pattern is defined as:

$$\Phi_4(\varphi) = \frac{1}{k_4}\left[\cos(b\sin\theta\sin\varphi) - \frac{q_{40}}{k_0} - \frac{q_{43}}{k_3}\cos(b\sin\theta\cos\varphi) + \frac{q_{30}q_{43}}{k_0k_3}\right] \quad \text{(A12)}$$

where:

$$q_{40} = \frac{\pi}{k_0}\int_0^{2\pi} E_1(b\sin\varphi)\,d\varphi$$
$$q_{41} = q_{42} = 0 \quad \text{(A13)}$$
$$q_{43} = \frac{\pi}{k_3}\int_0^{2\pi} E_1[2b\cos(\pi/4)\cos\varphi]\,d\varphi - \frac{q_{30}\pi}{k_0k_3}\int_0^{2\pi} E_1[b\cos\varphi]\,d\varphi$$

ACKNOWLEDGMENT

The authors would like to thank Prof. Antonis Kalis of Athens Information Technology for the fruitful discussions.

REFERENCES

1. Sibille, A., C. Oestges, and A. Zanella, *MIMO: From Theory to Implementation*, Chap. 10, Academic Press, Elsevier, 2011.
2. Chung, J.-Y., T. Yang, and J. Lee, "Low correlation MIMO antennas with negative group delay," *Progress In Electromagnetics Research C*, Vol. 22, 151–163, 2011.
3. Wallace, J. W. and M. A. Jensen, "Mutual coupling in MIMO wireless systems: A rigorous network theory analysis," *IEEE Transactions on Wireless Communications*, Vol. 3, No. 4, 1317–1325, 2004.
4. Waldschmidt, C., S. Schulteis, and W. Wiesbeck, "Complete RF system model for analysis of compact MIMO arrays," *IEEE Transactions on Vehicular Technology*, Vol. 53, No. 3, 579–586, May 2004.
5. Tsen, W.-F. and H.-J. Li, "Optimal impedance matching for capacity maximization of MIMO systems with coupled antennas and noisy amplifiers," *Progress In Electromagnetics Research C*, Vol. 15, 23–36, 2010.
6. Geyi, W., "Multi-antenna information theory," *Progress In Electromagnetics Research*, Vol. 75, 11–50, 2007.
7. Kalis, A., A. G. Kanatas, and C. Papadias, "A novel approach to MIMO transmission using a single RF front end," *IEEE Journal on Selected Areas in Communications*, Vol. 26, No. 6, 972–980, 2008.
8. Bains, R. and R. R. Müller, "Using parasitic elements for implementing the rotating antenna for MIMO receivers," *IEEE Trans. on Wireless Communications*, Vol. 7, No. 11, 4522–4533, November 2008.
9. Alrabadi, O., C. Papadias, A. Kalis, and R. Prasad, "A universal encoding scheme for MIMO transmission using a single active element for PSK modulation schemes," *IEEE Trans. on Wireless Communications*, Vol. 8, No. 10, 5133–5142, October 2009.
10. Barousis, V., A. G. Kanatas, and A. Kalis, "Beamspace domain analysis of single RF front-end MIMO systems," *IEEE Trans. on Vehicular Technology*, Vol. 60, No. 3, 1195–1199, March 2011.
11. Alrabadi, O. N., C. Divarathne, P. Tragas, A. Kalis, N. Marchetti, C. B. Papadias, and R. Prasad, "Spatial multiplexing with a single radio: Proof-of-concept experiments in an indoor environment with a 2.6-GHz prototype," *IEEE Communications Letters*, Vol. 15, No. 2, 178–180, February 2011.

12. Adams, A. T. and D. E. Warren, "Dipole plus parasitic element," *IEEE Trans. on Antennas and Propagation*, Vol. 19, 536–537, July 1971.
13. Harrington, R. F., "Reactively controlled directive arrays," *IEEE Trans. on Antennas and Propagation*, Vol. 26, No. 3, 390–395, May 1978.
14. Scott, N., M. O. Leonard-Taylor, and R. G. Vaughan, "Diversity gain from a single-port adaptive antenna using switched parasitic elements illustrated with a wire and monopole prototype," *IEEE Trans. on Antennas and Propagation*, Vol. 47, No. 6, 1066–1070, June 1999.
15. Ohira, T. and K. Gyoda, "Electronically steerable passive array radiator antennas for low-cost analog adaptive beamforming," *IEEE Int. Conf. Phased Array Syst. & Tech.*, 101–104, May 2000.
16. Iigusa, K. and T. Ohira, "A simple and accurate mathematical model of electronically steerable pa-rasitic array radiator antennas," *First IEEE Consumer Communications and Networking Conference, CCNC 2004*, 312–315, Jane 5–8, 2004.
17. Vaughan, R., "Switched parasitic elements for antenna diversity," *IEEE Trans. on Antennas and Propagation*, Vol. 47, No. 2, February 1999.
18. Barousis, V., A. G. Kanatas, A. Kalis, and C. Papadias, "A stochastic beamforming algorithm for ESPAR antennas," *IEEE Antennas and Wireless Prop. Letters*, Vol. 7, 745–748, 2008.
19. Sun, C., A. Hirata, T. Ohira, and N. C. Karmakar, "Fast beamforming of electronically steerable parasitic array radiator antennas: Theory and experiment," *IEEE Trans. on Antennas and Propagation*, Vol. 52, No. 7, July 2004.
20. Wennstrom, M. and T. Svantesson, "An antenna solution for MIMO channels: The switched parasitic antenna," *12th IEEE International Symposium on Personal, Indoor and Mobile Radio Communications, 2001*, Vol. 1, A-159–A-163, September 2001.
21. Kalis, A., A. G. Kanatas, M. Carras, and A. G. Constantinides, "On the performance of MIMO systems in the wavevector domain," *IST Mobile & Wireless Comm Summit*, Mykonos, Greece, June 5–8, 2006.
22. Sayeed, A. M., "Deconstructing multiantenna fading channels," *IEEE Trans. on Signal Processing*, Vol. 50, No. 10, 2563–2579, October 2002.
23. Tse, D. and P. Viswanath, *Fundamentals of Wireless Communication*, Chap. 7, Cambridge University Press, 2005.

24. Migliore, M. D., "On the role of the number of degrees of freedom of the field in MIMO channels," *IEEE Trans. on Antennas and Propagation*, Vol. 54, No. 2, February 2006.
25. Poon, A. S. Y., R. W. Brodersen, and D. N. C. Tse, "Degrees of freedom in multiple-antenna channels: A signal space approach," *IEEE Trans. on IT*, Vol. 51, No. 2, February 2005.
26. Bucci, O. M. and G. Franceschetti, "On the degrees of freedom of scettered fields," *IEEE Trans. on Antennas and Propagation*, Vol. 37, No. 7, July 1989.
27. Migliore, M. D., "On electromagnetics and information theory," *IEEE Trans. on Antennas and Propagation*, Vol. 56, No. 10, October 2008.
28. Miller, D. A., "Communicating with waves between volumes: Evaluating orthogonal spatial channels and limits on coupling strengths," *Applied Optics*, Vol. 39, No. 11, April 2000.
29. Proakis, J. G., *Digital Communications*, 4th edition, Chap. 4, 163, McGraw-Hill International Edition, 2000.
30. Van Trees, H. L., *Optimum Array Processing*, John Wiley & Sons, 2002.
31. Balanis, C., *Antenna Theory, Analysis and Design*, 3rd edition, Wiley, 2005.
32. Kermoal, J. P., L. Schumacher, K. I. Pedersen, P. E. Mogensen, and F. Frederiksen, "A stochastic MIMO radio channel model with experimental validation," *IEEE Journal on Selected Areas in Communications*, Vol. 20, No. 6, 1211–1226, August 2002.
33. Hu, Z., S. Sfar, and R. S. Blum, "Receive antenna selection for closely-spaced antennas with mutual coupling," *IEEE Trans. on Wireless Communications*, Vol. 9, No. 2, February 2010.
34. Mbonjo, H. N. M., J. Hansen, and V. Hansen, "MIMO capacity and antenna array design," *IEEE Global Telecommunications Conference*, Globecom, 2004.
35. Teal, P. D., T. D. Abhayapala, and R. A. Kennedy, "Spatial correlation for general distributions of scatterers," *IEEE Signal Processing Letters*, Vol. 9, No. 10, October 2002.
36. Olver, F. W. J., D. W. Lozier, R. F. Boisvert, and C. W. Clark, *NIST Handbook of Mathematical Functions*, National Institute of Standards and Technology (NIST) and Cambridge University Press, 2010.
37. Abouda, A. A. and S. G. Haggman, "Effect of mutual coupling on capacity of MIMO wireless channels in high SNR scenario," *Progress In Electromagnetics Research*, Vol. 65, 27–40, 2006.

38. Glazunov, A. A., M. Gustafsson, A. F. Molisch, F. Tufvesson, and G. Kristensson, "Spherical vector wave expansion of gaussian electromagnetic fields for antenna-channel interaction analysis," *IEEE Trans. on Antennas & Propagation*, Vol. 57, No. 7, July 2009.
39. Glazunov, A. A. and J. Zhang, "Some examples of uncorrelated radiation patterns for MIMO applications," *PIERS Proceedings*, 598–602, Marakkesh, Morocco, March 20–23, 2011.